CONF-760805--16

LA-UR -76-1115

TITLE: THE DIAMETER EFFECT IN HIGH-DENSITY HETEROGENEOUS EXPLOSIVES

AUTHOR(S): A. W. Campbell and Ray Engelke

SUBMITTED TO: 6th Symposium on Detonation

los alamos
scientific laboratory
of the University of California
LOS ALAMOS, NEW MEXICO 87544

Form No. 836
St. No. 2629
1/75

UNITED STATES
ENERGY RESEARCH AND
DEVELOPMENT ADMINISTRATION
CONTRACT W-7405-ENG. 36

THE DIAMETER EFFECT IN HIGH-DENSITY HETEROGENEOUS EXPLOSIVES*

A. W. Campbell and Ray Engelke
Los Alamos Scientific Laboratory
University of California
Los Alamos, New Mexico 87545

A phenomenological study of the dependence of steady detonation velocity on charge radius (the "diameter effect") in cylindrical configuration is described. Consideration is mainly given to high-density heterogeneous solid explosives cast or pressed to greater than 94% of theoretical maximum density. The work centers around a new fitting form which fits data for both homogeneous and heterogeneous explosives quite well. Some success is achieved in correlating the parameters of the fit with measured quantities. The effect of joints in rate sticks and of boosting on steady detonation velocity is examined experimentally. A significant joint effect is resolved. Finally, front-curvature measurements on a plastic bonded TATB are used to deduce the reaction-zone length for this explosive. Comparisons are made with zone lengths obtained by other methods.

INTRODUCTION

A study of the dependence of steady-state detonation velocity on charge radius in cylindrical geometry (the "diameter effect") is reported. Emphasis is placed on consideration of solid explosives which are heterogeneous (i.e., cast or pressed from a powder containing many different sizes of microcrystals) and at greater than 94% of theoretical maximum density (TMD). For purposes of comparison, diameter-effect curves of two liquid explosives are also included.

The diameter effect has importance at different levels. For example, it can be used as an engineering tool for gauging the size of system in which an explosive will behave "ideally." On a more basic level, the two-dimensional effects can be used as a probe for studying reaction-zone structure.

The theories of the diameter effect presented to date either have been shown to be incompatible with the experimental data for heterogeneous solid explosives [i.e., those of Eyring et al. (1) and of Jones (2)] or are not expressed in terms of the commonly measured experimental quantities [Wood and Kirkwood (3)]. The treatment given here is phenomenological; i.e., the study is restricted to finding regularities within the data. Such regularities should give hints on the mechanisms which are dominant and should act as a guide and constraint on a basic theoretical treatment. The work in this paper centers around a new fitting form which fits data for both homogeneous and heterogeneous explosives quite well. This form is applied to new data as well as to data taken from the literature.

In the course of obtaining the new experimental data, it was found that joints in small rate sticks perturbed the detonation velocity significantly for the purposes of high precision measurements. These results are discussed. A study was also made of the effect of boosting on the steady-state velocity. No significant effect was observed. Finally, measurements of front curvature were made on a plastic-bonded TATB. These measurements, when combined with the diameter-effect curve and the Wood-Kirkwood (WK) theory, determine a reaction-zone length on the central stream

*Work performed under the auspices of the Energy Research and Development Administration.

tube as a function of stick radius. The infinite-medium reaction-zone length thus obtained is compared with those from independent measurements.

I. EXPERIMENTAL

Explosives The explosives for which new data are presented were carefully prepared by casting or pressing following the procedures described by James (4). An exception was XTX-8003, which was composed of PETN mixed with a casting resin. This explosive was pressed into grooves cut in polycarbonate slabs and then the resin was allowed to polymerize. For this explosive, the densities of the rate sections were inferred from specimens with the same composition; for all other explosives, densities were obtained by immersion of the pieces used in the rate studies. In the case of Amatex/20, the pieces were sprayed with a thin film of plastic before immersion.

Detonation-Velocity Measurement Most of the rate measurements were made with the pin technique as described by Campbell et al. (5), except for a few changes of detail. All pieces were measured for length in a temperature-controlled room. The most common piece length was 50 mm, and lengths were measured to about 10^{-2} mm. The pieces were assembled in columns with 50-μm copper magnet wire inserted in the joints as ionization switches. The columns were then clamped as shown in Fig. 1. In order to ensure that joints between rate sections were closed and yet that the sections were not overcompressed, the clamping bolts were passed through carefully machined spacers as shown.

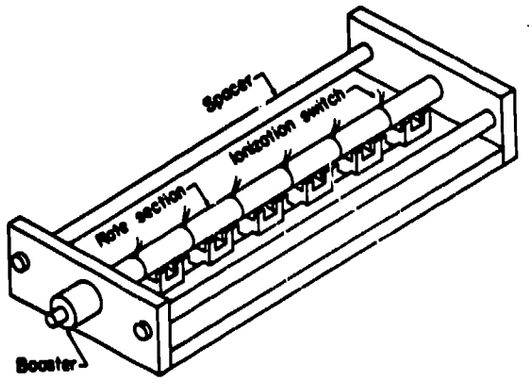

Fig. 1. Schematic of a typical rate-stick assembly.

In the case of PBX-9404 at diameters of about 1.3 mm and less, the detonation velocities were measured on individual pieces 12.7 mm long using a smear camera. As the result of carefully determining the image magnification and of dynamically calibrating the camera, the optical rate measurements are thought to be accurate to better than 0.1%.

Shots were temperature controlled to ± 1°C. Detonation velocities were obtained from the pin data by linear least-squares fitting.

II. DIAMETER EFFECT

Figure 2 shows the dependence of the steady-state detonation velocity on the reciprocal of the charge radius for the group of explosives considered. One notes that numerous scales and shapes are present. Except for the liquids (nitromethane and TNT) and for pressed TNT and XTX-8003, all the data necessary to generate these curves were obtained without confinement. The curves for all the solid explosives (except the TATB formulations) show downward concavity. It was shown by Malin et al. (6) using data for Composition B, that this type of curvature is contrary to the theory of Eyring et al. (1) and is not fitted properly by Jones' theory (3). It should be noted that Eyring's theory does fit the data for (the homogeneous explosives) liquid nitromethane and liquid TNT quite well. The WK theory (3) cannot be tested against the data because the velocity decrement is expressed in terms of the detonation-wave curvature on the central stream tube rather than in terms of the stick radius.

In view of these failings or inapplicability, it was decided that a phenomenological approach should be made and that the objective of this approach would be to find regularities in the data. Such an approach, if successful, should give hints to, and place constraints on, a correct hydrodynamic theory of the effect. In addition, it would systematize the data and allow accurate velocity interpolations to be made at any desired diameter.

The cornerstone of this treatment is the functional form.

$$D(R) = D(\infty)\,[1 - A/(R-R_c)], \quad (1)$$

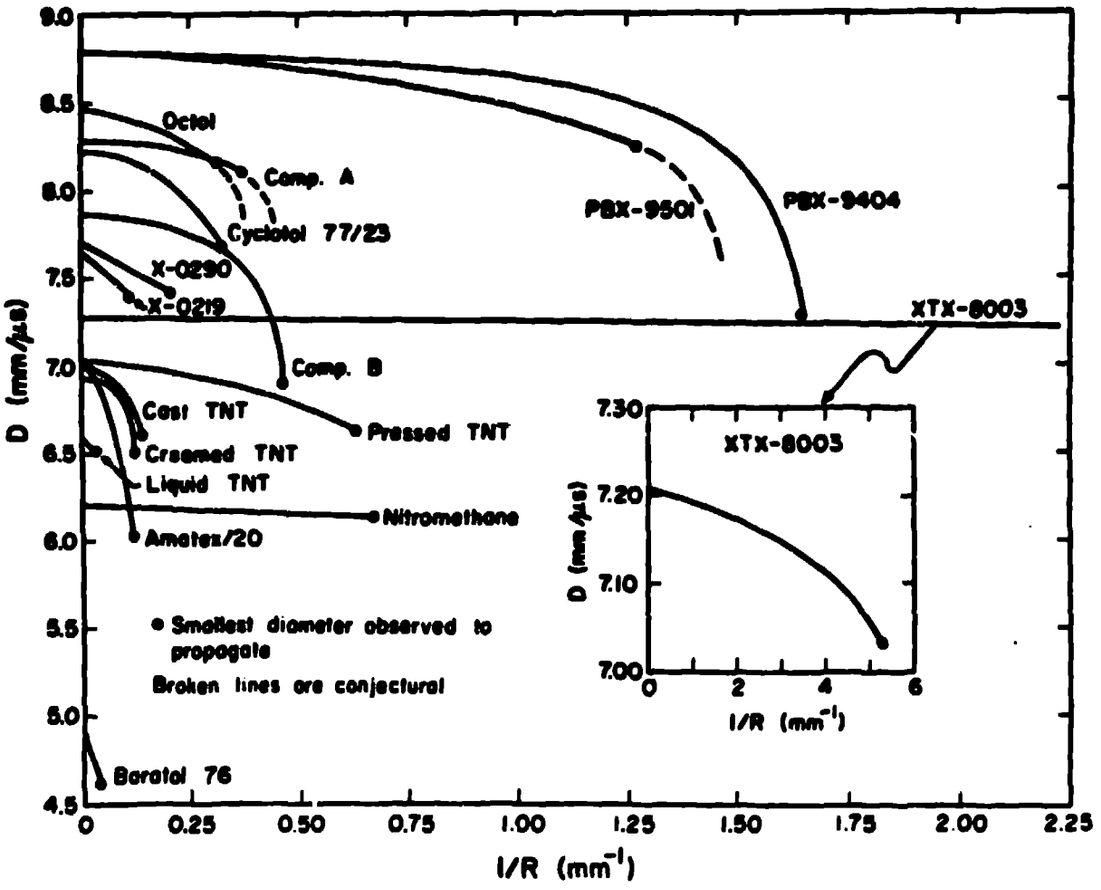

Fig. 2. Composite of diameter-effect curves in the D-vs-1/R plane. Broken lines are conjectural.

where D(R) and D(∞) are the detonation velocities at charge radius R and in infinite medium, respectively, and A and R_c are length parameters. An alternate form of Eq. (1), which displays the non-Eyring part explicity is

$$D(R) = D(\infty)\left\{[1-A/R] - \frac{AR_c}{R(R-R_c)}\right\}. \quad (2)$$

Note that Eqs. (1) and (2) reduce to Eyring's form where $R_c \to 0$. This is a reasonable behavior since a line in the D-vs-1/R plane accurately represents the data at sufficiently large charge diameter. In addition, as $R \to R_c$, $D(R) \to -\infty$; i.e., there is an asymptote at finite R. At fixed R_c, the parameter A determines how abruptly the downturn in the curve occurs; i.e., the smaller the value of A, the more abrupt the drop. Figure 3 displays this. Since $D(R) \to -\infty$ as $R \to R_c$, the physical region corresponds to values of $R > R_c$ and in particular the failure radius must obey $R_f > R_c$.

Equation (1) was fitted to the available data by the method of least squares. Graphical displays of typical fits are given in Figs. 4 and 5. The results of the fits are given in Table I. The PBX-9404 result shown in Fig. 4 is typical of high-density heterogeneous explosives. Contrasting behavior is shown by the liquid form of nitromethane (7) and of TNT (8).

The liquid TNT data are linear in the D-vs-1/R plane. The fit of the nitromethane data shows slight upward

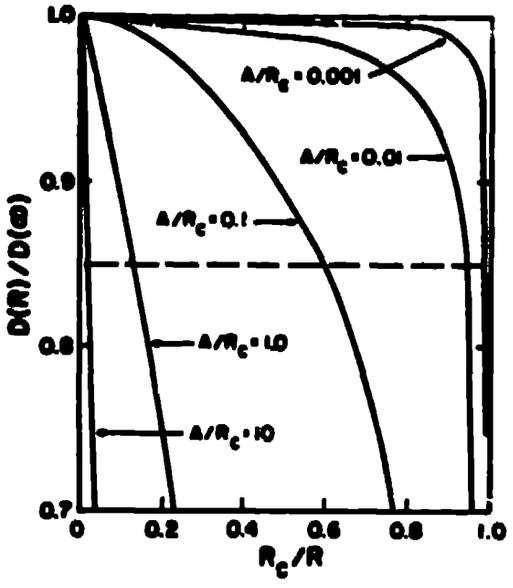

Fig. 3. Parametric dependence of the diameter-effect curve. The hashed line represents the approximate position of the maximum observed velocity deficit.

concavity, which is expressed mathematically by R_c having a value less than zero. The TNT formulations are exceptional in the sense that of all the solid explosives treated they are the only ones which show linear diameter-effect curves. There is a hint of upward concavity in the data, but the least-squares analysis shows that R_c is not significantly different from zero.

It should be mentioned that the fit for PBX-9404 is unsatisfactory in that

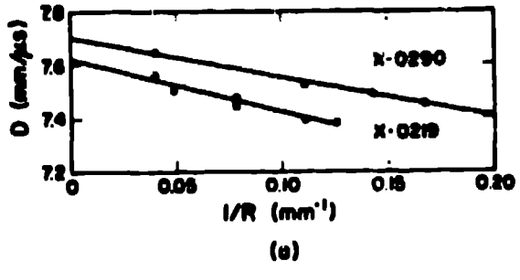

(a)

Fig. 5a. Diameter-effect curves for X-0290 (ρ = 1.895 g/cm^3) and X-0219 (ρ = 1.915 g/cm^3).

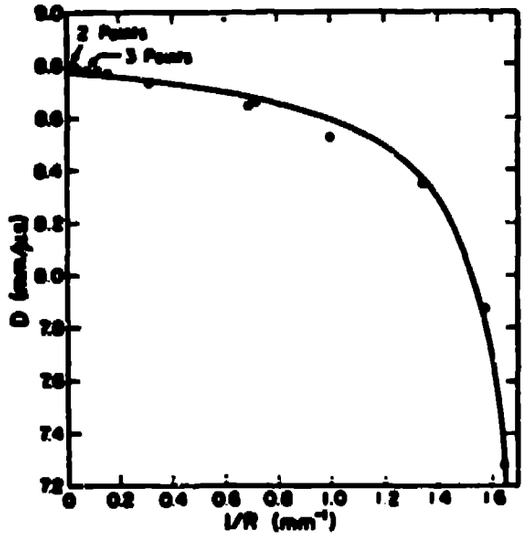

Fig. 4. Diameter-effect curve for PBX-9404; ρ = 1.8-6 g/cm^3.

the deviations about the fit are larger than what is believed to be the experimental error in measuring the detonation velocity. It is not known whether this is a shortcoming in the fitting form or is due to some uncontrolled variable in the explosive itself; e.g., particle-size variations (6). The latter explanation cannot be ruled out, because the data for PBX-9404 were accumulated over a long period of time, i.e., approximately 19 years. The deviation about the fits

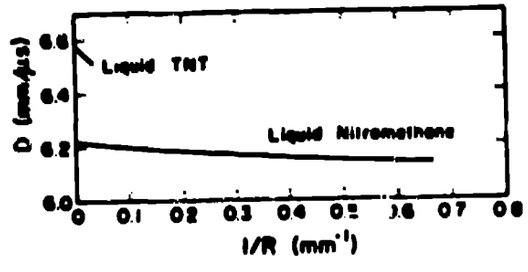

(b)

Fig. 5b. Diameter-effect curves for liquid TNT (ρ = 1.443 g/cm^3) and liquid nitromethane (ρ = 1.128 g/cm^3). The liquid TNT data points all lie within 0.4 m/s of the fit. The liquid nitromethane points all lie within 2 m/s of the fit.

TABLE I

DIAMETER-EFFECT PARAMETERS

Explosive	Data Points[a] (No./diam)	Density/TMD (g/cm³)	% TMD[b]	$D(\infty) \pm \sigma_D$ (mm/μs)	$R_c \pm \sigma_{R_c}$ (mm)	$(A \pm \sigma_A) \times 10^3$ (mm)	Expt. Failure Radius[c] (mm)	Comment
Liquid Nitromethane	9/5	1.128/1.128	100	6.213 ± 0.001	-0.0 ± 0.1	2.6 ± 0.2	1.42 ± 0.21	Ref. (9). The fit shows slight upward concavity. Shots fired in brass tubes with 3.18 mm thick walls.
Liquid TNT	11/6	1.443/1.443	100	6.574 ± 0.001	0.0	29.1 ± 0.6	31.3 ± 1.3	Ref. (8). R_c fixed at 0.0 gives the smallest variance of fit. Shots fired in pyrex tubes with 1.56-mm thick walls.
XTX-8003	58/6	1.53/1.556	98.3	7.260 ± <0.001	0.111 ± 0.001	0.191 ± 0.001	0.18 ± 0.05	Ref. (10). 80/20 PETN/silicone rubber. Fired in half-cylinder configuration confined in polycarbonate.
Composition A	5/5	1.687/1.700	99.	8.274 ± 0.003	1.2 ± 0.1	1.39 ± 0.17	<1.1	Ref. (6). 92/8 RDX/Wax. No sizes that failed were reported.
Composition B	16/12	1.700/1.742	97.6	7.859 ± 0.011	1.94 ± 0.07	2.84 ± 0.19	2.14 ± 0.03	[illegible]
PBX-9404	16/13	1.846/1.865	99.0	8.776 ± 0.017	0.951 ± 0.004	0.89 ± 0.08	0.59 ± 0.03	[illegible]
PBX-9501	7/5	1.832/1.855	98.8	8.802 ± 0.004	0.48 ± 0.07	1.9 ± 0.1	<0.76	Unpublished LASL data. 95/2.5/1.25/1.25 HMX/Estane/BDNPA/BDNPF
Octol	8/6	1.814/1.843	98.4	8.481 ± 0.007	1.34 ± 0.21	6.9 ± 0.9	<3.2	Ref. (11). 77/23 HMX/TNT
Cyclotol 77/23	8/8	1.740/1.755	99.1	8.210 ± 0.014	2.44 ± 0.12	4.89 ± 0.82	3.0 ± 0.6	77/23 RDX/TNT [illegible]
Baratol 76	3/3	2.619/2.63	99.6	4.874	4.36	102	21.6 ± 2.5	[illegible] Data [illegible] three-point fit. The curve is not well enough defined near failure to properly test the R_c vs R_f correlation.
Amatex/20	6/6	1.613/1.710	94.3	7.030 ± 0.010	4.4 ± 0.2	99. ± 3.	8.5 ± 0.5	Ref. (12). Composition is nominally 20/40/40 RDX/TNT/AN. The AN median particle size was ≈ 0.5 mm.
X-0219	8/6	1.915/1.946	98.4	7.627 ± 0.015	0.0	86.9 ± 2.3	7.5 ± 0.5	Unpublished LASL data. 90/10 TATB/Kel-F 800. When R_c is freed a statistically insignificant result R_c = -5. ± 6. mm is obtained. See the nitromethane result.
X-0290	5/5	1.895/1.942	97.6	7.706 ± 0.009	0.0	19.4 ± 0.6	4.5 ± 0.5	Unpublished LASL data. 95/5 TATB/Kel-F 800. When R_c is freed a statistically insignificant result R_c = -1.6 ± 0.8 mm is obtained. See the nitromethane result.
Creamed TNT	5/5	1.615/1.654	97.6	6.942 ± 0.020	7.01 ± 0.26	5.67 ± 1.87	7.3 ± 1.0	Ref. (13).
Pressed TNT	*20/8	1.62/1.654	97.9	7.045 ± 0.17	0.57 ± 0.21	6.1 ± 1.3	1.31 ± 0.28	Ref. (14) Confined in cellophane tubes with 0.05-mm thick walls.
Cast TNT	*15/5	1.62/1.654	97.9	6.999 ± 0.011	5.5 ± 0.3	11.3 ± 1.7	7.25 ± 0.25	Ref. (14).

[a] Number of shots that propagated a steady wave/number of distinct diameters at which observations were made.

[b] Theoretical maximum density.

[c] R_f is the average of the radii from two go/no-go shots; σ_f is defined as one-half the difference in the go/no-go radii.

of Fig. 5 are of the same size as the experimental error. This is also true of the other fits listed in Table I.

It is thought that the very different conformation of the curves shown in Figs. 4 and 5 is due to there being two mechanisms supporting wave propagation in heterogeneous solids, i.e., hot spots and homogeneous burn; while in homogeneous explosives only homogeneous burn is present. Thus, one can speculate that in heterogeneous explosives at large diameter both mechanisms contribute to driving the wave while at diameters near failure only the hot-spot mechanism sustains wave motion. The lack of a region of sharp drop in the liquid curves is then due to the absence of the hot-spot mechanism.

The quality of the fits obtained with Eq. (1) can be gauged from Fig. 6. In that figure, the fitting form and some typical data points for the various explosives are plotted in a reduced coordinate plane, (i.e., $D(R)/D(\infty)$ vs $A/(R-R_c)$. The existence of a plane in which all the data can be plotted near a single curve is suggestive that the processes which control the diameter effect are identical and that the different curves in the D-vs-1/R plane result from variations of the relative effectiveness of the processes.

Another observation that can be made is that the fitting parameter R_c correlates with the experimental failure radius. This correlation is shown in Fig. 7. One sees that except for Amatex/20 and Baratol 76 (not plotted), the linear least-squares fit $R_c = (0.877 \pm 0.054)R_f$ passes close to the data. The Baratol 76 curve is questionable because it is determined by only three points and none of these are very close to the failure diameter. Consequently, the curvature may not be sufficiently well determined for the fit to be useful near failure. Of the other explosives which give data points markedly to the right of the fitting curve, cast TNT, Amatex/20, and Octol may be expected to yield small charges containing critically insensitive regions—cast TNT by variation in the freezing rate, Amatex/20 by segregation of ammonium nitrate, and Octol by virtue of the large-particle-size HMX used. These insensitive regions may have resulted in larger values of R_f.

An attempt was made to correlate A with R_f. This was not as successful. The data scatter badly about a power law of the form $(A = KR_f^n)$. However, although one cannot quantitatively relate A and

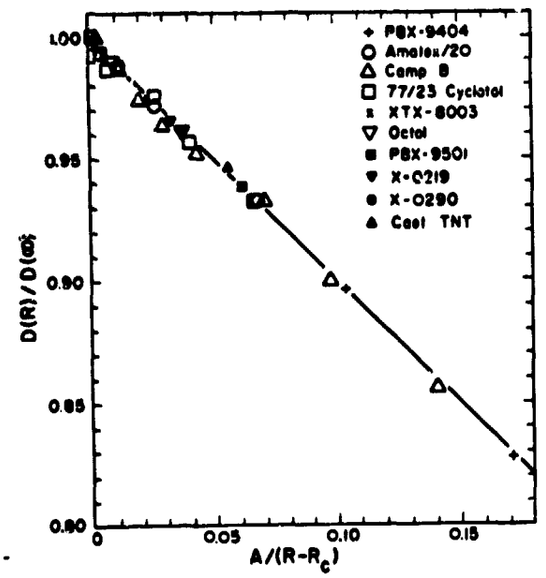

Fig. 6a. Diameter-effect curve and data points in reduced coordinates over the full range of velocity deficit.

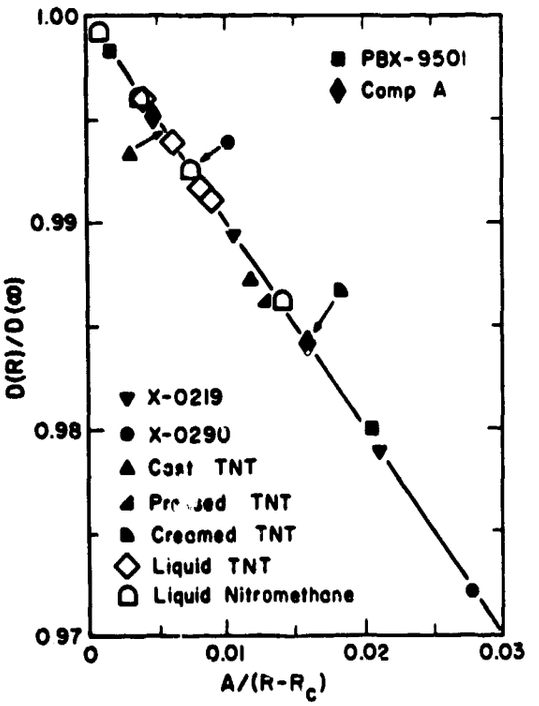

Fig. 6b. Diameter-effect curve and data points in reduced coordinates over the first 3% of velocity deficit.

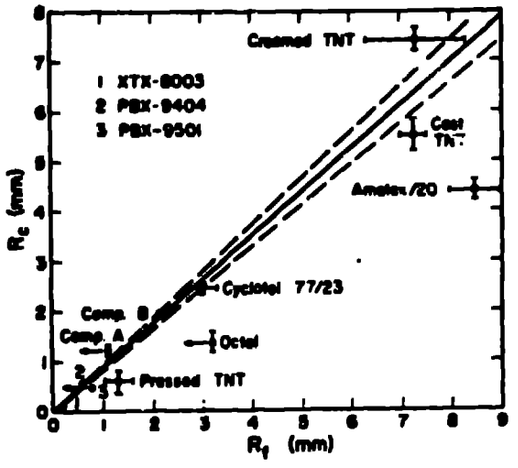

Fig. 7. Correlation between R_f and R_c. The hashed lines correspond to plus or minus one standard deviation of the slope of the line. Where no error bars are indicated they are less than the dot size; where error bars are indicated they are those of Table I. The equation of the straight line is $R_c = (0.877 \pm 0.054)R_f$. An arrow to the left of an entry indicates that no sticks that failed were fired.

R_c, there is a correlation in the sense that a larger value of A tends to correspond to a larger value of R_f.

III. THE JOINT EFFECT

It is necessary to fire very small rate sticks (≈1-mm diam) in order to obtain a complete diameter-effect curve for some of the explosives in Table I. One has the intuitive feeling that the presense of joints and pins in such sticks may significantly perturb the detonation wave trajectory. Such an effect (called the "joint effect") would result in underestimation of detonation velocity and overestimation of failure diameter. These considerations prompted a search for such an effect.

The experimental method was to record with a smear camera the progress of a detonation wave in a rate stick consisting of 4 to 6 cylindrical segments of the same diameter. The explosive was in the form of right-circular cylinders machined to size from singly-pressed billets. The cylinders ranged in length from 25.4 mm to 12.7 mm, and in diameter from 5.01 mm to 1.5 mm. Because PBX-9501 is a rather compliant explosive, the charges having diameters of 1.5 and 2 mm were measured on a contour projector with digital readout.

Each piece was supported at two places and was tied to a cradle with 50-μm copper wire to prevent buckling of the column under pressure. Boostering consisted of a small pellet of PBX-9404 initiated by a detonator which was held in a threaded mount. Good contact was secured at the joints between cylinders by inserting a thin metal shim in one of the joints and tightening the threaded detonator adaptor nut until slight friction was felt upon sliding the shim. The shim was then removed and the nut turned an amount calculated to advance the detonator a distance equal to the thickness of the shim.

The assembled rate stick was mounted before the smear camera with a precision magnification scale and a photographic resolution chart attached to the cradle. To ensure constant magnification along the stick, the whole assembly was arranged perpendicularly to the optic axis by use of a laser beam projected along the camera optical axis and reflected from the magnification scale.

When charge alignment was achieved, photographic resolution was checked on still photographs made on Panatomic-X film. Allowance was made for any deviation between the plane of the magnification scale and the surface of the rate stick by moving the camera axially an appropriate distance. Temperature was controlled to 23° ± 1°C.

Before firing the rate stick, the film was lightly fogged by rotating the mirror with the shutter open; a break in the camera slit produced a line indicating the writing direction along the film, and in the analysis of the firing record the writing speed at the location of the record was interpolated from a previous calibration.

Where pin records were taken, the switches were made of silver ribbon 3 mm wide by 10 μm thick. These were inserted in joints between stick segments and held in place with Eastman 910 adhesive.

The experimental space-time trajectories were fitted to the model

$$x(t) = B + Dt + \delta N, \qquad (3)$$

where N is the segment number on the stick (0, 1, 2, ...), δ is the spatial

joint effect, D is the detonation velocity, t is the time measured from some origin, β is the intercept at N = 0 and t = 0, and x(t) is the position of the detonation at time t. The assumptions of the model are that the detonation velocity is the same in the steady part of each segment and that there is an identical offset (possibly zero) at each joint.

Figure 8 shows the type of behavior to be expected from the model and the experiment if there is a significant joint effect. Figure 9 shows the results for PBX-9501 in terms of the time lag at a joint (i.e., δ/D). One sees that the effect is a strong function of stick diameter for the three sticks fired with clean-butt joints.

Furthermore, the one stick fired with glue and pin foils present in the joints shows a greatly enhanced effect.

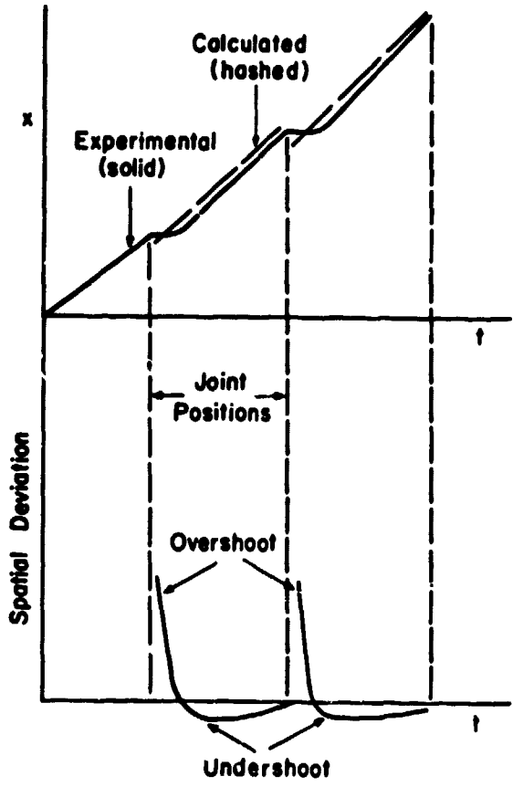

Fig. 8. Schematic of experimental and calculated detonation trajectories are shown in the upper portion. Anticipated deviations of experimental points about the model are shown in the lower portion.

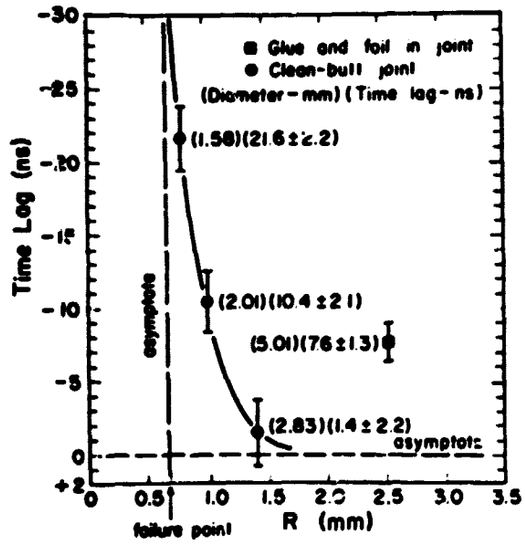

Fig. 9. Joint-effect for PBX-9501 as a function of stick radius and form of the joint. The position of the vertical asymptote is conjectural. The error bars correspond to one standard deviation

In this case, the error induced in the pin measurement of velocity due to the joint perturbations was ±0.2% (17 m/s).

One concludes that if one wishes to make highly precise measurements of detonation velocity or of failure diameter this effect must be avoided.

IV. BOOSTER EFFECT

There were indications in the work of Bdzil (15) that the steady-state velocity in a rate stick might be a function of the manner of boosting. If such an effect were present, some of the diameter-effect data would have to be reinterpreted. Since Bdzil's work was concerned with PBX-9404 and since the deviations about the fit were non-random for this explosive, it was decided that an experimental test should be made. This was done by strongly over- and underdriving two very long PBX-9404 rate sticks.

The explosive consisted of 30 carefully machined right-circular cylinders, 25.4 mm diameter by 50.8 mm long, taken from two pressed billets. Density was measured for each piece by immersion in water. The uniformity of the billets

was illustrated by the results: 7 pieces had densities of 1.845 g/cm³, 20 pieces 1.846 g/cm³, and 3 pieces 1.847 g/cm³.

These cylinders were randomized between two rate sticks, one of 13 pieces to be overboosted and one of 17 pieces to be underboosted. Underboosting was achieved by use of an Amatex/20 column 25.4 mm in diameter and 152 mm long. (The detonation pressure of Amatex/20 in plane geometry is ≈200 kbar.) Overboosting of the shorter stick was obtained by use of the booster diagramed in Fig. 10. (The design of this booster was due to B. G. Craig and produced a pressure of 404 kbar in PBX-9404.)

Wave curvature was measured at the end of each stick by means of a small mirror which was oiled and clamped to the terminal surface. Light from a small shocked-argon light source was reflected into a smear camera so as to produce an extinction record of the arrival of the detonation wave.

Precautions were taken with temperature control, film shrinkage, space resolution, camera writing speed, image magnification, and many other factors.

No large effect on the detonation velocity was observed; the measured velocities were 8.7735 ± 0.0004 and 8.7754 ± 0.0003 mm/μs for the overdriven and underdriven sticks, respectively. Note that the velocity results are not within two standard deviations of each other. The (central) front curvatures were measured and they were significantly different being 337 ± 3 mm (overdriven) and 355 ± 4 mm (underdriven). The larger velocity corresponds to a longer radius of curvature, as it should. It is unexpected that the overdriven stick shows a smaller radius of curvature and a lower detonation velocity.

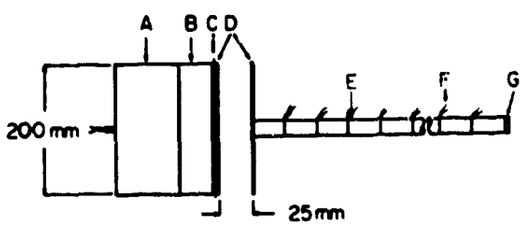

Fig. 10. Diagram of overboosted rate stick assembly.

A. Plane-wave lens
B. 50.8-mm PBX-9404
C. 0.38-mm polyethylene
D. 0.25-mm magnesium
E. Rate sections
F. 0.05-mm copper wire switches
G. Mirror

V. FRONT CURVATURE AND REACTION-ZONE LENGTH IN X-0219

Front-curvature measurements were made on X-0219 (90/10 TATB/KelF 800) at stick diameters of 18, 25.4, and 50.8 mm. It was found that the detonation fronts near the charge axis are quite accurately represented by spherical waves. The three values of front curvature on the stick axis fall close to a straight line in the front-curvature-vs-stick-radius plane. The combination of detonation-velocity and front-curvature measurements allows one to calculate the reaction-zone length on the stick axis as a function of stick radius, if the WK theory (3) is accepted as valid.

In Fig. 11, the radius of curvature (S) is plotted vs the stick radius (R). From the limited amount of available data, one finds an approximately linear relationship between S and R. The curvatures were obtained by fitting a spherical wave model by the method of least squares to the central 50% of the end traces.

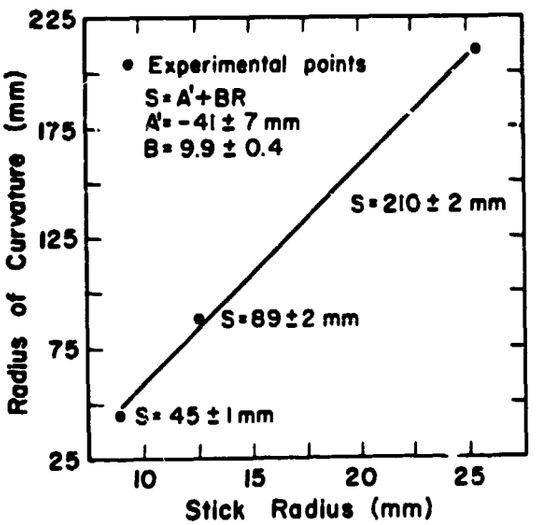

Fig. 11. Central front curvature vs stick radius for X-0219 rate sticks.

The WK relationship for the velocity decrement is

$$D(S) = D(\infty)\left[1 - a\xi^*(S)/_S\right], \quad (4)$$

where D(S) and D(ξ) are the detonation velocities with radii of curvature S and ∞, respectively, a is a constant dependent on the properties of the explosive, and $\xi^*(S)$ is the reaction-zone length on the stick axis.

It should be noted that the WK result has builtin assumptions more appropriate for a homogeneous explosive than for a heterogeneous one. This may be less of a deficiency for X-0219 than for other solid heterogeneous explosives, because TATB formulations exhibit some liquid-like behavior, e.g., linear diameter-effect curves, small velocity deficits before failure, and temperature dependent failure diameter.

Combining the diameter-effect curve, $D(R) = D(\infty)[1 - A/R]$, where $D(\infty) = 7.627 \pm 0.015$ mm/us and $A = 0.269 \pm 0.023$ mm with the front-curvature relationship $S = A' + BR$, where $A' = -41 \pm 7$ mm and $B = 9.9 \pm 0.4$ gives the form

$$D(S) = D(\infty)\left[1 - \left(\frac{BA}{S - A'}\right)/S\right]. \quad (5)$$

Comparison of Eq. (5) with Eq. (4) allows one to make the identification

$$\xi^*(S) = \frac{BA}{a}\, S/(S - A') \quad (6)$$

or alternately

$$\xi^*(R) = \frac{A}{a}\left[B + A'/R\right]. \quad (7)$$

By use of the experimental values $P_{CJ} = 278$ kbars, $P_{spike} = 364$ kbars, $\rho = 1.915$ g/cm³, $D = 7.627$ mm/us, and a Y-J-W equation of state, one finds that a=2. Since A, a, and B are greater than zero and A' is less than zero, Eq. (7) represents a straight line in the ξ^*-vs-1/R plane with negative slope. This shows that the axial reaction-zone length (distance from shock to sonic locus) decreases with decreasing charge radius. A decrease in charge radius results in an increase in axial flow divergence and, as a result, the sonic plane moves closer to the shock. The intercept, given by AB/a, is the infinite-medium reaction-zone length and it has the numerical value $\xi^*(\infty) = 1.3$ mm. The result is compared in Table II with reaction-zone lengths obtained by independent means.

One notes that the measurements given in Table II break into two classes, i.e., those for zone lengths greater or less than 1 mm. It is felt that the first three entries are superior estimates. Consequently, it is asserted that the reaction-zone is abnormally long in some TATB formulations and of the order of 1 mm.

TABLE II

REACTION-ZONE LENGTHS FOR TATB FORMULATIONS

Technique	Reaction-Zone Length (mm)	Formulation (wt%)	Density (g/cm³)	% TMD	Reference
Wood-Kirkwood theory and axial front curvature measurements	1.3	90/10 TATB/KelF 800	1.911-1.915	98.20-98.41	This paper
Raytrace acoustics and PHERMEX rarefaction-wave experiment	5.	90/5/5 TATB/Bᵗwax/Elvax	1.74	99.32	Ref. (16)
Magnetic probe measurement	3.3	95/5 TATB/KelF 800	1.895	97.58	W.C.Davis this symposium
Pushing inert plates of various thicknesses	0.3	90/10 TATB/KelF	1.915	98.41	Ref. (17)
Eyring theory and diameter-effect curve measurements	0.14	90/10 TATB/KelF 800	1.911-1.915	98.20-98.41	This paper

ACKNOWLEDGMENTS

The high quality of the explosives used was due to the careful work of many individuals at Groups WX-3 and WX-2, especially A. Popolato, J. L. Parkinson, H. L. Flaugh, and M. J. Urizar. The integrity of the field work was due to the competent efforts of J. A. Montoya, J. E. LaBerge, and K. O. Humphreys. We are obligated to N. E. Langley for technical photographic support. We thank J. R. Travis and J. B. Bdzil for helpful discussions.

REFERENCES

1. H. Eyring, R. E. Powell, G. H. Duffy, and R. B. Parlin, Chem. Rev. 45, 69 (1949). Also see R. B. Parlin, C. J. Thorne, and D. W. Robinson, Tech. Rept. No. 1, Institute for the Study of Rate Processes, University of Utah, (1952).

2. H. Jones, Proc. Roy. Soc. (London) A189, 415 (1947).

3. W. W. Wood and J. G. Kirkwood, J. Chem. Phys. 22, 1920 (1954).

4. E. James, Jr., 2nd ONR Symposium on Detonation, p. 1 (1955).

5. A. W. Campbell, M. E. Malin, T. J. Boyd, Jr., and J. A. Hull, 2nd ONR Symposium on Detonation, p. 18 (1955).

6. M. E. Malin, A. W. Campbell, and C. W. Mautz, 2nd ONR Symposium on Detonation, p. 360 (1955).

7. A. W. Campbell, M. E. Malin, and T. E. Holland, 2nd ONR Symposium on Detonation, p. 336 (1955).

8. E. A. Igel and L. B. Seely, 2nd ONR Symposium on Detonation, p. 320 (1955).

9. M. E. Malin, Los Alamos Scientific Laboratory, unpublished data, 1955.

10. L. E. Hatler, Los Alamos Scientific Laboratory, unpublished data, 1974.

11. C. W. Mautz, Los Alamos Scientific Laboratory, unpublished data, July 1956.

12. A. Popolato, LA-5711-PR, p. 8 (1974). This work was performed with funds provided by the Defense Advanced Research Projects Agency under DARPA Order No. 2502.

13. W. B. Cybulski, W. Payman, and D. W. Woodhead, Proc. Roy. Soc. 197, 71 (1948).

14. L. N. Stesik and L. N. Akimova, Russ. J. Phys. Chem. (Eng. trans.) 33, 148 (1959).

15. J. B. Bdzil, Los Alamos Scientific Laboratory, personal communication, April 1974.

16. R. Engelke and W. C. Davis, Bull. Am. Phys. Soc. 15, 1483 (1975).

17. B. G. Craig, Los Alamos Scientific Laboratory, personal communication, June 1975.